Thin Film Morphologies of ABC Triblock Copolymers Prepared from Solution

Hubert Elbs,[†] Clarissa Drummer,[‡] Volker Abetz,[§] and Georg Krausch*,[†]

Lehrstuhl für Physikalische Chemie II and Bayreuther Zentrum für Kolloide und Grenzflächen (BZKG), Bayreuther Institut für Makromolekülforschung (BIMF), and Lehrstuhl für Makromolekulare Chemie II, Universität Bayreuth, 95440 Bayreuth, Germany

Received October 3, 2001

ABSTRACT: We have studied the thin film morphologies of polystyrene-*b*-poly(2-vinylpyridine) diblock copolymers and polystyrene-*b*-poly(2-vinylpyridine)-*b*-poly(*tert*-butyl methacrylate) triblock copolymers after "annealing" in the vapor of different solvents. We find distinct differences in the resulting thin film morphologies. The differences are explained qualitatively on the basis of concentration-dependent Flory−Huggins interaction parameters of the different components.

Introduction

The microdomain structure in block copolymer thin films has recently attracted increasing attention both experimentally and theoretically.[1−23] These investigations are typically motivated either by the inherent interest in phase equilibria in confined geometry or by the potential use of the well-ordered structures for lithographic applications.[24−26] The resulting morphologies are determined by a complex interplay of different parameters including the molecular properties of the polymers (interaction parameters, molecular weight, molecular architecture), the interfacial interactions at the boundary surfaces, and the film thickness. Often the preparation process leads to the formation of (metastable) structures that do not represent the melt equilibrium but are induced for example by selectivity of the solvent.[27] Though not in equilibrium, such structures often exhibit high regularity and may be of particular interest for patterning applications as they significantly increase the number of patterns to be created by a given polymer. An in-depth understanding of the formation of such nonequilibrium structures, however, is difficult as it requires knowledge of the properties of the polymer solutions (solubility and interaction parameters as a function of solvent concentration) and control over the solvent extraction process (e.g., solvent extraction rates).[28]

In the present paper, we describe recent experiments on thin films of an AB diblock and an ABC triblock copolymer formed under different preparation conditions. We will show that quite different thin film structures are formed after solvent extraction depending on the nature of the solvent and on the solvent extraction rate. In particular, we demonstrate that proper control of the preparation conditions enables reproducible production of a rich variety of novel thin film morphologies.

Experimental Section

For the present experiments, we used monodisperse batches of a polystyrene-*block*-poly(2-vinylpyridine) diblock copolymer (M_w = 140 kg/mol, φ_S = 0.14, φ_V = 0.86) and a polystyrene-*block*-poly(2-vinylpyridine)-*block*-poly(*tert*-butyl methacrylate) (SVT) triblock copolymer (M_w = 110 kg/mol, φ_S = 0.17, φ_V = 0.26, φ_T = 0.57). In the following, we refer to the two polymers as $S_{14}2VP_{86}$ and $S_{17}2VP_{26}tBMA_{57}$, respectively. The polymers were synthesized by anionic polymerization. Details of the synthesis have been described elsewhere.[29] Solvents (chloroform and tetrahydrofuran; p.a.) were purchased from Merck and used as obtained.

Thin films were deposited onto polished silicon wafers[30] by dip coating from chloroform solution. After drying, the films were exposed to tetrahydrofuran (THF) vapor or chloroform vapor to induce mobility and allow microphase separation to occur. Both solvents are good solvents for all three polymer components. To control the solvent vapor treatment process quantitatively, the samples were kept at a constant temperature of T_p = 24 °C in a closed vessel together with a reservoir of pure solvent, which was kept at a lower temperature ranging between T_s = 5 and 23.8 °C. By a variation of the solvent temperature T_s, the vapor pressure could be varied. In turn, the degree of swelling of the polymer films could be quantitatively adjusted. In-situ spectroscopic ellispometry measurements were used to quantify the solvent concentration in swollen films at any given vapor pressure.

After drying, the films were investigated with optical microscopy (OM), scanning force microscopy (SFM), and scanning electron microscopy (SEM). OM images were taken on a Zeiss Axiotech optical microscope. SFM images were taken on a Digital Instruments Dimension 3100 microscope operated in TappingMode. Secondary electron SEM images were taken on a field emission SEM (LEO 1530) using the in-lens detector at a low accelerating voltage of 0.8 kV. Under these conditions the potential contrast between the different components of the block copolymers can be resolved. However, the first measurements were taken on samples that were stained in OsO_4 vapor for 3 min to enhance the contrast between the different components.

Results

THF Vapor Annealing. We start our discussion with the films annealed in THF vapor. The films were exposed to a vapor pressure of $p = 0.94p_0$ (p_0 being the vapor pressure of saturated THF vapor at room temperature). According to the ellipsometric measurements, this treatment swells the films to about twice their dry thickness ($\Phi_P \approx 0.44$). Subsequently, the films were dried at a controlled solvent extraction rate by reducing the THF vapor pressure over a time interval of 4 days from $p = 0.94p_0$ to $p = 0.3p_0$ by a linear reduction of

[†] BZKG.
[‡] BIMF.
[§] Lehrstuhl für Makromolekulare Chemie II.
* Corresponding author: e-mail georg.krausch@uni-bayreuth.de.

10.1021/ma011734e CCC: $22.00
Published on Web 06/04/2002

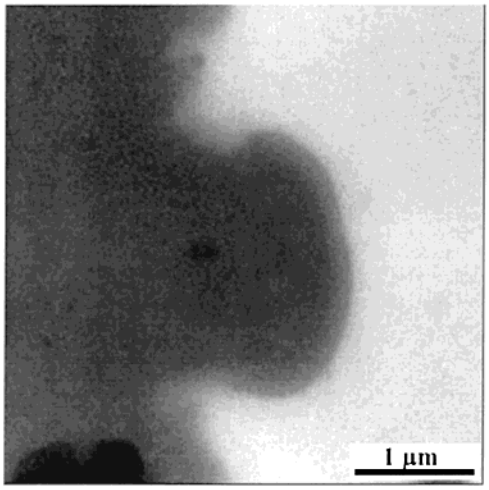

Figure 1. SFM images (TappingMode height images) of a $S_{142}VP_{86}$ film after treatment in THF vapor (reduction of vapor pressure from $p = 0.94p_0$ to $p = 0.3p_0$ over 4 days; height scale $\Delta z = 0-100$ nm).

the temperature of the solvent reservoir. The final vapor pressure corresponds to a polymer concentration of about $\Phi_P = 0.9$, which is above the vitrification concentration. Therefore, further reduction of the vapor pressure will not lead to an additional change of the morphology, at least on a time scale of minutes or shorter. (The latter was checked on samples exposed to THF vapor at $p = 0.58p_0$ (corresponding to $\Phi_P \approx 0.78$) over a period of 1 day, where no change in morphology was observed.) In this way a slow drying process resembling the typical preparation of bulk samples is realized.

After solvent extraction the samples were removed from the vapor chamber and examined with optical microscopy, SFM and SEM. Optical microscopy (not shown here) indicates that the films of both $S_{142}VP_{86}$ and $S_{172}VP_{26}tBMA_{57}$ form terraced surface structures; i.e., different lateral regions exhibit different, yet well-defined, film thickness. This finding indicates that microphase separation has occurred, and microdomain structures were formed, which align parallel to the plane of the film.[2] SFM was used to determine the step heights and to reveal the in-plane structure of the terraces on a molecular length scale.

For films of the diblock copolymer $S_{142}VP_{86}$ we find a step height of $\Delta d = 60-70$ nm. The surfaces of the terraces do not show any lateral structures (Figure 1), indicating the formation of lamellae aligned parallel to the plane of the film.

For films of the triblock copolymer $S_{172}VP_{26}tBMA_{57}$ the height differences between the terraces amount to $\Delta d = 53 \pm 3$ nm. Figure 2a shows an SEM image of the surface of such a film. In the left half of the image (denoted by "B"), the surface looks rather smooth and featureless. The film thickness in this area was determined by SFM and amounts to 5 ± 1 nm. It is likely that this part of the film is a polymer brush, i.e., a thin, laterally homogeneous layer of polymer chains physisorbed from solution via the polar P2VP block.[31]

Figure 2a shows the transition from this polymer brush to a first terrace (denoted by "1"). In the first terrace (Figure 2a,b) one finds a striped surface pattern. The composition of the copolymer suggests an interpretation of this pattern as a core−shell cylinder morphology with a PS core and a P2VP shell embedded in a PtBMA matrix. This assumption is further corroborated by the lateral periodic variation of the stripe size, which is found at the transition from the first to the second terrace (Figure 2b). This variation is consistent with laterally shifted, horizontal core−shell cylinders. Figure 2c shows an SEM image of a hole in the second terrace which gives access to the underlying first terrace. The stripes in the lower terrace are shifted laterally relative to the stripes on the top terrace by half of the lateral period. This is an additional indication of a hexagonal array of core−shell cylinders aligned parallel to the plane of the film.

The lateral period between neighboring cylinders was determined by SFM and SEM and amounts to $L = 63 \pm 2$ nm (SFM) and $L = 64 \pm 2$ nm (SEM), respectively. For a hexagonal array of cylinders one expects an interlayer spacing $d = \sqrt{3}/2\ L \approx 55 \pm 2$ nm. This value is in very good agreement with the step height $\Delta d = 53 \pm 3$ nm determined from SFM measurements. This agreement is an additional confirmation of a hexagonal core−shell cylinder morphology.

We note that the SFM and SEM images are also consistent with what usually is referred to as the cylinder at cylinder morphology of ABC triblock copolymers.[32] In this morphology the B middle block does not form a continuous shell around the minority component core but rather breaks up into separate cylinders of smaller diameter which arrange symmetrically at the surface of the core. On the basis of the experimental data, we cannot exclude this structure; however, it would imply a *perfect* alignment of the middle block cylinders with respect to the plane of the film. For a clear distinction between the two morphologies cross-sectional transmission electron microscopy (TEM) would be desirable. Unfortunately, we were not able to remove the films from the substrates after solvent vapor annealing for cross-sectional TEM imaging.

For bulk samples of the $S_{172}VP_{26}tBMA_{57}$ triblock copolymer slowly cast from THF solution hexagonal structures were reported, too.[29] The bulk long period L_{bulk} was determined by small-angle X-ray scattering (SAXS) to $L_{bulk} = 67$ nm, corresponding very well to the respective thin film values. We note, however, that an unambiguous interpretation of the bulk TEM data proved difficult. Actually, hexagonally perforated lamellae (with 67 nm distance between neighboring perforations and a lamellar spacing of 50 nm) were considered as a structural model; however, core−shell cylinders seem to be in agreement with the data as well. No indication for a cylinder at cylinder morphology was reported. We note, though, that the particular structure formed in a bulk piece of material does not necessarily coincide with the structure of an ultrathin film, where interfacial and confinement effects cannot be neglected. Anyhow, bulk experiments generally suffer from the problem of multiple domains with random orientations with respect to the slice cut for TEM inspection. In contrast, the thin film experiments are more straightforward as the domains spontaneously align with respect to the boundary surfaces. This advantage becomes even more pronounced when several morphologies coexist.

For the $S_{172}VP_{26}tBMA_{57}$ triblock copolymer annealed in THF vapor we indeed observe the "coexistence" of different morphologies. Aside from the striped pattern described above, in some regions of the film a pattern of bright stripes is observed, which appear connected

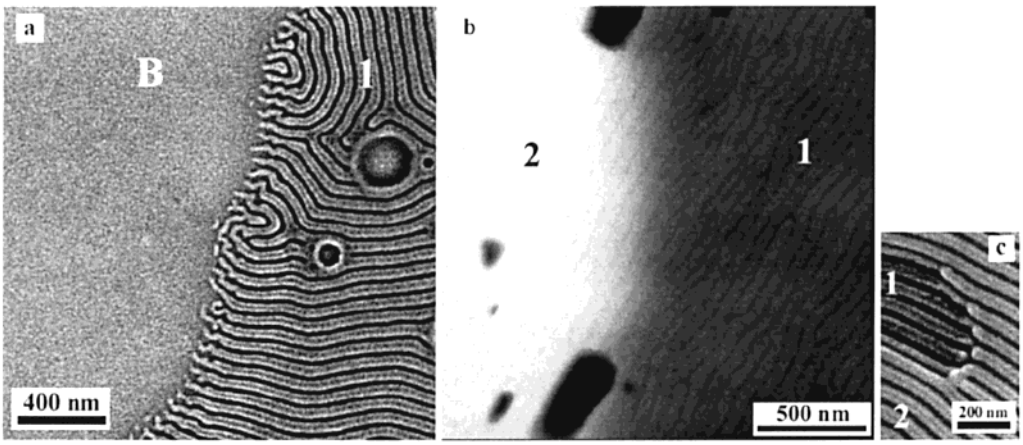

Figure 2. SEM images (a, c) and SFM image (height scale $\Delta z = 0-60$ nm) (b) of an $S_{17}2VP_{26}tBMA_{57}$ film after vapor annealing in THF. (a) shows the transition between the physisorbed brush layer (B) to the first layer of cylinders (1). (b) shows the transition from the first to the second layer of cylinders. (c) shows a defect in the second layer which gives access to the underlying first layer.

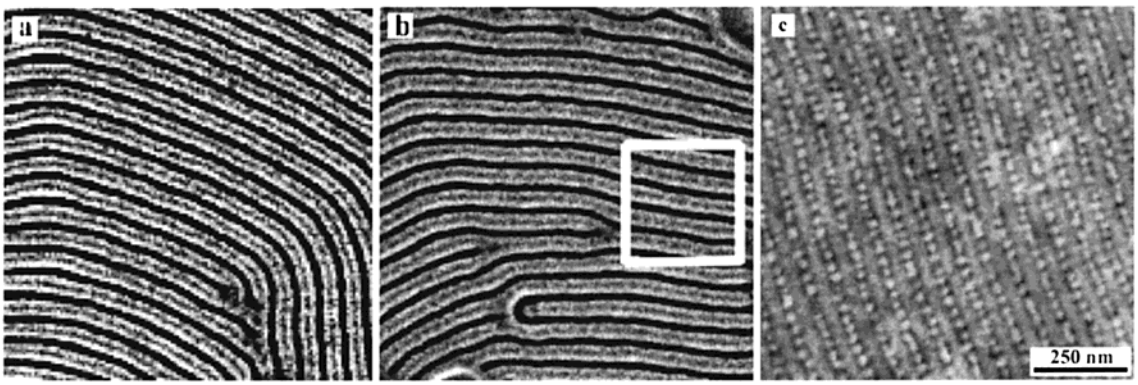

Figure 3. SEM images (a, b) and SFM image (height scale $\Delta z = 0-10$ nm) (c) of the first layer of cylinders on a thin film of $S_{17}2VP_{26}tBMA_{57}$. (a) shows a core−shell morphology. (b) and (c) show regions characterized by a sphere/cylinder morphology.

by perpendicular bright "bridges" (see white box in Figure 3b). This morphology may best be explained as a modified core−shell structure, where the PS core breaks up into isolated PS microdomains (gray) embedded within a P2VP cylinder (bright) (Figure 5b). A more distinct image of this morphology is the SFM image displayed in Figure 3c. To best of our knowledge, no bulk morphology of this type ("sphere in cylinder") was yet observed in ABC triblock copolymers.

Figure 4a shows yet another morphology which appears in certain areas of what may be considered the first layer of cylinders (first terrace). The SEM image shows a herringbone-like structure where a central stripe is crossed by sloped bright stripes. This morphology may be interpreted as a helix around cylinder morphology.[32,33] Here, cylinders of the middle block wind around the minority core like a helix. This morphology was first observed in bulk experiments on polystyrene-*block*-polybutadiene-*block*-poly(methyl methacrylate) (PS-*b*-PB-*b*-PMMA) triblock copolymers in a narrow composition window.[32] In our case, cylindrical PS cores (gray) would be surrounded by helices of P2VP (bright), embedded in a matrix of PtBMA (dark).

From the SEM images we find that the nearest-neighbor distance between cylinders in the helix around cylinder morphology ($L = 56 \pm 2$ nm) is considerably smaller than in the sphere in cylinder morphology ($L = 62 \pm 2$ nm) and the core/shell morphology ($L = 64 \pm 2$ nm). The pitch of the helices amounts to 36 ± 2 nm; the distance between the spheres within a cylinder is 34 ± 2 nm.

We concentrate in the following on the helix around cylinder morphology. For comparison, in Figure 4b we display a TEM image of a PS−PB−PMMA triblock copolymer, which forms the cylinder/helix structure in the bulk.[32] The bulk sample shows a more or less random distribution of the two chiralities. Moreover, in bulk the chirality in some cases seems to change even along a single cylinder. This points to the problem of cutting artifacts in bulk TEM (the slice used for TEM imaging may run across a single cylinder, thereby "exposing" its top and bottom sides) and indicates that an unambiguous determination of the chirality is hardly possible in the bulk. In contrast, in the thin film a single layer of cylinders is formed which nicely aligns with respect to the substrate plane. Therefore, no cutting artifacts occur and the helicity can unambiguously be determined. Three remarkable observations are made: At first, the helical structure is only observed for a film thickness corresponding to a single layer of cylinders. We were not able to find helical structures in thicker regions of the films. Second, the helicity is found to strictly alternate between neighboring cylinders within the plane, which may be compared to the alternating orientation of magnetic spins in an antiferromagnetic material. For simplicity, we will call the order of the alternating helicities of our block copolymer "antiferromagentic", although the material does not show any

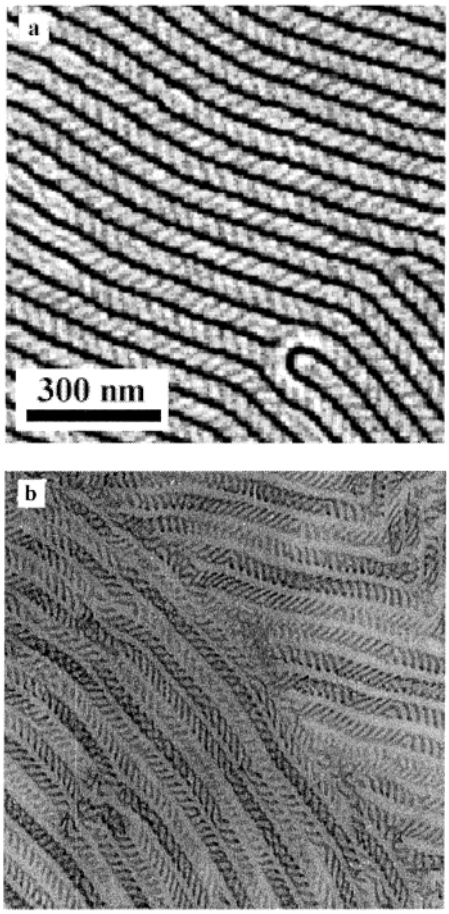

Figure 4. (a) SEM image of the first layer of cylinders of a thin film of $S_{17}2VP_{26}tBMA_{57}$ after THF vapor treatment. The surface structure indicates a helix/cylinder morphology.[33] (b) TEM cross section of a bulk sample of a $S_{26}B_{12}$ M_{62} triblock copolymer (M_W = 218 000 g/mol).[32]

magnetic behavior. Finally, the helicity does not change along a single cylinder except if the cylindrical lattice itself exhibits a defect. In the latter case (see lower left corner in Figure 4c), the helicity along a couple of neighboring cylinders changes in such a way that irrespective of the defect the antiferromagnetic superstructure is preserved.

The antiferromagnetic superstructure of the helices together with the observation that the S-cylinders appear to be somewhat closer packed in the case of the helical morphology points to packing arguments responsible for the observed effects. Indeed, two screws of same pitch but opposite helicity can be fit tightly together while this is not possible for screws of same helicity (see Figure 5a). Consequently, the observation of a strictly alternating helicity of neighboring cylinders yields a closer packing possibly releasing unfavorable chain stretching. Therefore, the average distance between neighboring cylinders is smaller in the helical superstructure as compared to the core−shell cylinders. From these considerations, one would expect the antiferromagnetic superstructure to be a favorable morphology in the bulk as well. It must be realized, however, that a strict alternation of helicity is possible only in a two-dimensional array, i.e., if individual helices have two nearest neighbors only. In the hexagonal arrangement of cylinders present in the bulk, strict alternation between nearest neighbors is impossible, and the antiferromagnetic superstructure is frustrated. Indeed, while multilayers of core−shell cylinders are found in thicker regions of the films, no indication of two or more layers of helices is observed in our experiments.

Summarizing the observations after "annealing" in THF vapor, we note that thin films of the $S_{14}2VP_{86}$ diblock copolymer exhibits a lamellar morphology while the $S_{17}2VP_{26}tBMA_{57}$ triblock copolymer shows three different cylindrical morphologies: core−shell cylinders (or cylinders at cylinders), spheres in cylinders, and helices around cylinders. The respective morphologies are sketched in Figure 5b. The core−shell cylinder structure arises from the sphere in cylinder morphology by merging the isolated PS spheres into a continuous PS cylinder. Accordingly, it arises from the helix around cylinder morphology by merging P2VP helices to complete P2VP shells around the PS cylinders. Small fluctuations in density or concentration may already suffice to induce transitions between these "neighboring" morphologies. In addition, potential impurities by PS homopolymers or PS−P2VP diblock copolymers may be a possible reason. Such impurities cannot be completely excluded, although no hint was found in GPC measurements of the triblock copolymer. Finally, the "coexistence" of different cylindrical morphologies indicates that the films have not yet reached their equilibrium structure (i.e., the equilibrium structure of the concentrated polymer solution just above the highest vitrification concentration) during preparation. We note that thermal annealing after the vapor treatment did not lead to any significant changes of the observed morphologies.

Chloroform Vapor Annealing. Figure 6 shows SFM images of a film of the $S_{14}2VP_{86}$ diblock copolymer after a treatment with chloroform vapor. The vapor pressure was reduced from $p = 0.94p_0$ to $p = 0.3p_0$ within 1 day. According to the ellipsometric measurements, this corresponds to an increase of polymer concentration from about $\phi_P = 0.37$ to $\phi_P = 0.83$. For small film thicknesses one finds a stepped surface and a striped surface morphology with a long period of $L = 76 \pm 2$ nm (Figure 6a). The step heights amount to $d = 39 \pm 5$ nm. At film thicknesses larger than some 150−200 nm one finds a coexistence of a striped morphology ($L = 76 \pm 2$ nm) and a hexagonal structure ($L = 75 \pm 2$ nm) (Figure 6b). Presumably, the diblock copolymer forms a cylindrical morphology with PS cylinders embedded within a matrix of P2VP. The structures of the thinner films can be interpreted as layers of cylinders aligned parallel to the substrate whereas in thicker films cylinders with perpendicular orientation may coexist with layers of cylinders with parallel orientation.

Figure 7 shows SEM images of the $S_{17}2VP_{26}tBMA_{57}$ triblock copolymer after annealing in chloroform vapor. Here, the vapor pressure was reduced from $p = 0.94p_0$ to $p = 0.3p_0$ within 4 days. Some regions show a pattern of isolated points of local hexagonal or rhombic symmetry (Figure 7a). The average distance between neighboring points amounts to $L = 69 \pm 2$ nm. Other regions of the film show a regular structure of sinusoidally shaped lines, which include two shifted rows of points (Figure 7b). The distance between the sinusoidal lines amounts to 176 ± 2 nm and between the rows of points 51 ± 3 nm, and the periodicity along the sinusoidal lines is 109 ± 3 nm.

For comparison, in Figure 8 we show a simulation of the 112 plane of the cubic unit cell of the double-gyroid morphology.[34] One can recognize a wave structure with the same symmetry as in Figure 7b. In contrast to the

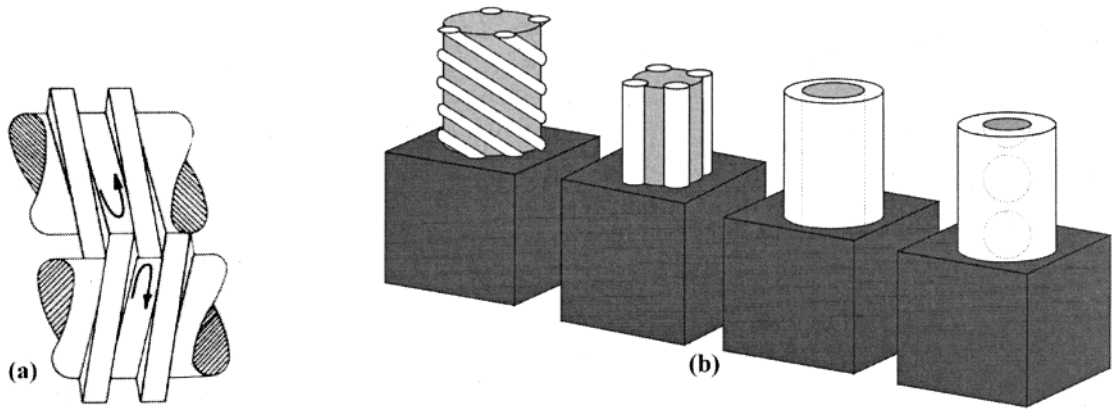

Figure 5. (a) Sketch of two screws with opposite chirality fitting tightly into each other. (b) Sketch of the different cylindrical morphologies observed on $S_{17}2VP_{26}tBMA_{57}$ thin films after THF vapor treatment. The color code was chosen as to match the gray values observed in the SEM experiments (PS, gray; P2VP, bright; PtBMA, dark).

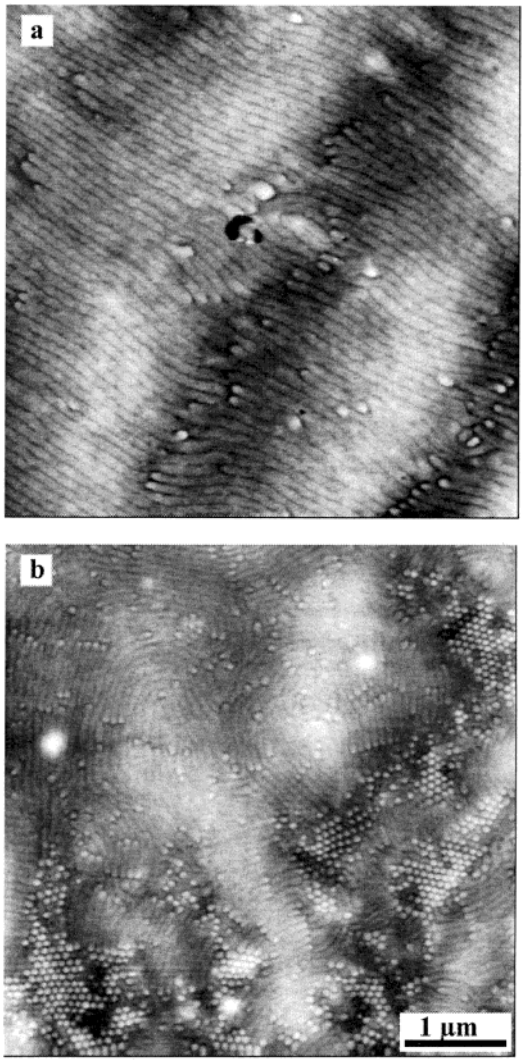

Figure 6. SFM images of a $S_{14}2VP_{86}$ film after vapor treatment in chloroform.

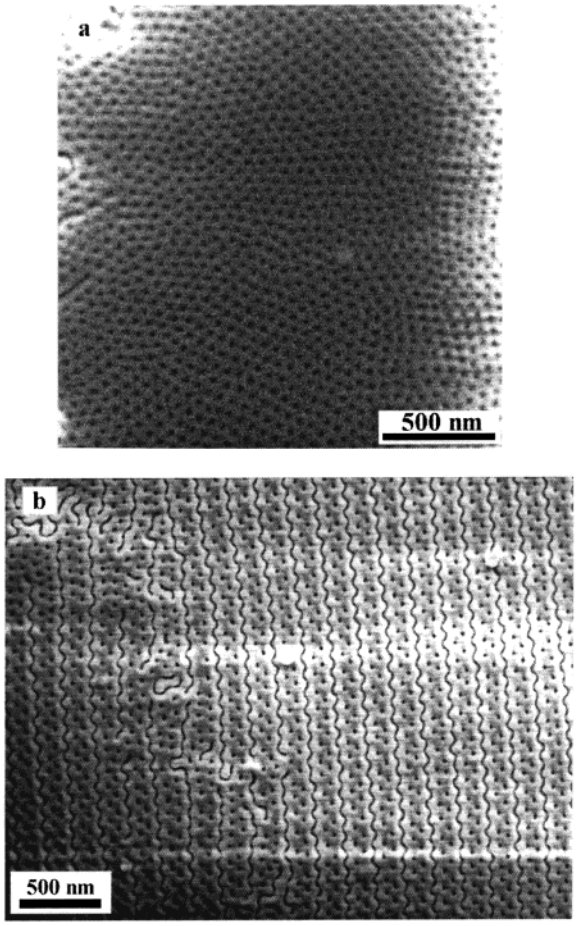

Figure 7. SEM images of a $S_{17}2VP_{26}tBMA_{57}$ film after vapor treatment in chloroform.

SEM image, the simulation result does not include points, though. However, the arrangement of the points in the SEM image corresponds to the arrangement of the extrema of the stronger kinked waves in the simulation. Possibly, the observed morphology can be interpreted as a core−shell double-gyroid aligned with the surface parallel to its (112) plane.[42] It may coexist with an array of core−shell cylinders aligned perpendicular to the plane of the film. In either case, the structures would have a PS core surrounded by a shell of P2VP embedded in a matrix phase of PtBMA. The net structure of the double gyroid in the simulation is depicted dark. So the waved lines and the points in Figure 7b would be formed by the minority components PS and P2VP. As for the alignment of this structure relative to the boundary surfaces, we note the epitaxial relation between the (112) plane of the gyroid and the (100) plane of the lamellar phase and the (01) plane of the hexagonal phase.[41] Given that both hexagonal phases and lamellar phases tend to align with the respective planes parallel to the boundary surfaces in

Figure 8. Simulation results of the (112) plane of the cubic unit cell of the double-gyroid morphology.[34]

thin films, it does not come as a surprise that a similar behavior is found for a thin film with gyroid structure.

Various Evaporation Rates. In a next step the dependence on the evaporation rate was checked. To this end the preparation process of films of the $S_{17}2VP_{26}tBMA_{57}$ triblock copolymer from THF solutions was varied. Again, the films were exposed to a THF vapor with a vapor pressure of $p = 0.94p_0$. But this time the vapor pressure was reduced to $p = 0.3p_0$ in only 15 min or 3.5 h. Figure 9 shows SFM images of the corresponding surface morphologies.

After the 15 min preparation the film exhibits terraces as after the 4 days preparation (height of the first terrace, 26−27 nm; second, 43−44 nm). The microstructure does not show a cylindrical symmetry, though. In the terraces one finds a rather disordered micellar structure (Figure 9a) with an average lateral periodicity of 67 ± 3 nm.

The 3.5 h preparation results in a noncylindrical morphology as well. The SFM image in Figure 9b shows regions with a hexagonal wagon-wheel structure (A) (average distance of the triangle centers 40 ± 3 nm) and regions with a rhombic (almost hexagonal) arrangement of rings (B) (average distance 79 ± 2 nm). An unambiguous identification of the phases in the SFM image is not possible without additional information as no clear material contrast between the components is observed. The wagon-wheel structure is known from literature to be characteristic for a bicontinuous morphology,[35,36] and a simulation of the 110 plane of the double-gyroid morphology yields rhombic (almost hexagonally) arranged rings.[34] Therefore, the observed morphology can presumably be interpreted as a bicontinuous gyroid morphology. Given the composition of the block copolymer, a core−shell double gyroid with two networks of PS with P2VP shells and a matrix of PtBMA may be anticipated.

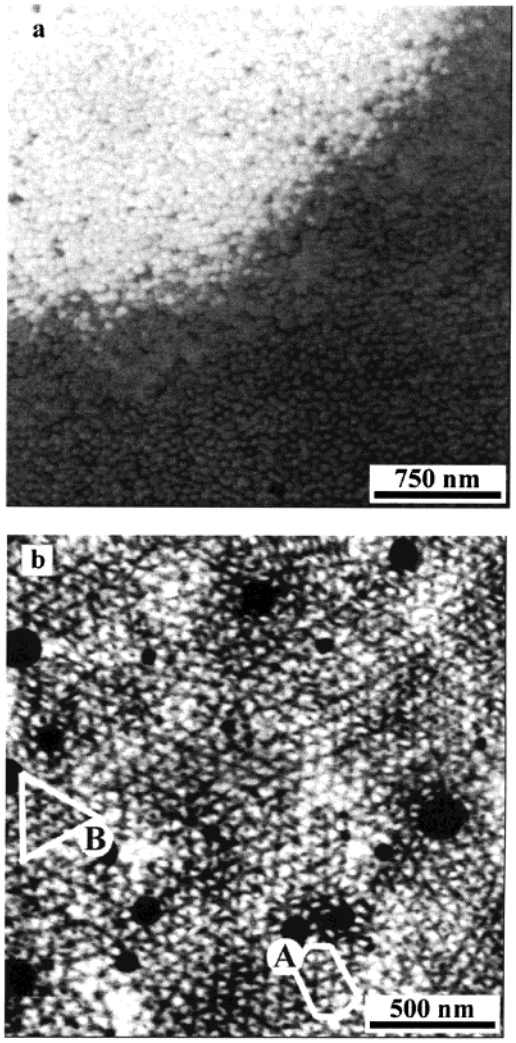

Figure 9. SFM images of a $S_{17}2VP_{26}tBMA_{57}$ film after treatment in THF vapor: reduction of vapor pressure from $p = 0.94p_0$ to $p = 0.3p_0$ over 15 min (a) or 3.5 h (b).

Discussion

The above results show a distinct dependence of the resulting thin film morphologies on the preparation conditions, in particular the nature of the solvent and the solvent extraction rate. Despite its asymmetry, the diblock copolymer $S_{14}2VP_{86}$ forms a lamellar structure after treatment with THF vapor. After a treatment with chloroform vapor it forms cylinders, a morphology with larger interface and larger mean curvature. The triblock copolymer $S_{17}2VP_{26}tBMA_{57}$ forms a cylindrical structure after THF vapor treatment and after treatment with chloroform vapor a morphology with a lower mean curvature and a morphology with the symmetry of a gyroid.

On first sight this behavior is surprising, as both THF and chloroform are good solvents for the three polymers PS, P2VP, and PtBMA. If the effect of the solvents would simply be a dilution of the different microphases, one would expect the slow drying process to lead to the same morphology irrespective of the solvent. In symmetric diblock copolymers a disorder−order transition leads from a mixed phase directly to an ordered phase with lamellar morphology,[37] and a further increase of concentration does not change the morphological symmetry. For asymmetric block copolymers, however, besides an order−disorder transition (ODT) also different order−order transitions (OOTs) can occur during a change of the concentration.[38,39] If the time scale of microdomain rearrangement at the OOT is larger than the experimental time scale of solvent removal, the low-concentration morphology may be frozen during sample preparation. Accordingly, if these time scales are different in different solvents, this may lead to different morphologies after drying.

As the solvent was evaporated very slowly (large experimental time scale), the solvent dependence of the

morphology may rather be due to specific interactions. Comparing the relative degrees of swelling of the constituent homopolmyers in the two solvents by ellipsometry, we find that THF is rather nonselective, while chloroform shows a weak selectivity for P2VP. Therefore, the phase diagrams of the respective block copolymer solutions are expected to be slightly different. From systematic ellispometric measurements on both homopolymers and binary random copolymers of the three polymers,[40] we estimate the interaction parameter $\chi_{PS/P2VP}$ to be positive in the relevant concentration regime ($\Phi_P = 0.44-0.9$), indicating a repulsive interaction of the components. Thus, a lamellar conformation with a small contact area between these two components and with a small mean curvature is preferred. A lamellar structure may be further stabilized by the external interfaces with SiO_x attracting the P2VP blocks and the free surface attracting the PS blocks.

In the presence of chloroform, on the other hand, $\chi_{PS/P2VP}$ is found to be negative at low concentrations and increases only at about $\phi_P = 0.7-0.75$ to similarly high positive values as in THF.[40] In addition, P2VP exhibits better solubility in chloroform and therefore should be swollen more than PS. Thus, at least up to a concentration of $\phi_P = 0.7$ the cylindrical morphology should be favored over the lamellar morphology. A transition at high concentrations may be kinetically inhibited due to proximity to the vitrification concentration.

Finally, the ellispometric measurements[40] indicate that the interaction parameter $\chi_{PS/PtBMA}$ is positive both in THF and in chloroform. Therefore, PS tends to microphase separate from the other components even at lower concentrations in chloroform, where the interaction parameter $\chi_{PS/P2VP}$ is negative. The values of the interaction parameter $\chi_{PtBMA/P2VP}$ indicate only a weak incompatibility of these two polar polymers in THF, while a stronger incompatibility is expected in chloroform. This could explain the observation of a morphology with larger mean curvature (cylinders) after treatment with THF and a smaller mean curvature morphology (gyroid) after treatment with chloroform vapor.

In addition to a solvent dependence the morphology of the $S_{17}2VP_{26}tBMA_{57}$ films annealed with THF vapor shows a clear dependence on the solvent extraction rate. After extraction in 15 min the films exhibit a micellar structure, after extraction in 3.5 h a bicontinuous morphology, and after extraction in 4 days a cylindrical morphology.

During the evaporation of the solvent the concentration of the polymer solution increases. At lower concentrations the relaxation time is short enough for the system to reach the thermodynamic equilibrium. At higher concentrations the relaxation time of the polymer solution will eventually reach the time scale of the preparation process, and the respective morphology will be frozen. Thus, as the interaction parameters, the volume ratios, and the degree of phase separation strongly depend on the concentration, it is not surprising that different solvent extraction rates yield different morphologies. Different extraction rates will interrupt the dynamic development of the morphology from a region of weak separation at lower concentrations to a region of strong separation at different (unknown) concentrations. The results indicate that the morphology in thin films of $S_{17}2VP_{26}tBMA_{57}$ triblock copolymers exhibits a development from a micellar structure through a bicontinuous morphology to a cylindrical morphology with increasing polymer concentration.

According to the ellispometric measurements,[40] the interaction parameter $\chi_{PtBMA/P2VP}$ between PtBMA and P2VP at $\Phi = 0.5$ is rather small. It may therefore be anticipated that these two blocks form a mixed phase, and only the PS blocks are phase separated. The micellar structure could then be interpreted as spheres or cylinders of PS in a P2VP/PtBMA matrix. The interaction parameter is expected to incease with increasing concentration, which in turn leads to phase separation of the P2VP and PtBMA blocks and to core−shell cylinders at higher concentrations.

It is not clear whether the observed morphologies are really thermodynamically stable at certain intermediate concentrations or induced by the specific dynamics of the preparation process. To answer this question, additional experiments with very fast extraction rates but different values for the initial vapor pressure are planned. In this way one should be able to freeze the morphologies at different concentrations, provided that the fast extraction of the solvent does not lead to a considerable change of the symmetry of the morphology. Perhaps such experiments clarify the development of the bicontinuous morphology at intermediate extraction rates which cannot be explained by the concentration dependence of the interaction parameters.

Conclusion

In conclusion, we have investigated the thin film structures of asymmetric AB diblock and ABC triblock copolymers after solvent vapor annealing in different solvents. We find distinct differences in the resulting structures depending on the solvent used for vapor annealing and the solvent extraction rate. The differences can be qualitatively understood on the basis of the different swelling behavior of the respective blocks in the two solvents.[40] Obviously, after solvent removal the films do not reach their melt equilibrium structure. However, since the glass transition temperatures of all components are far above room temperature, the resulting structures have long-term "stability". Therefore, they may be useful for lithographic applications, for example.

Although we are far from an in-depth understanding not to mention predictability of the observed morphologies, the results indicate the importance of well-controlled preparation conditions. Moreover, some insight into the various interaction parameters and their concentration dependence can prove helpful in "understanding" the observed results. Even though the results at present are still rather descriptive, we feel that they represent a step forward in controlling and understanding microdomain formation in the presence of solvents. Given the high viscosities of many complex architecture block copolymers the use of solvents can hardly be circumvented. Therefore, we expect that an experimental (and theoretical) approach to such metastable nonequilibrium structures will be of importance in future work on the steadily increasing number of complex block copolymers accessible through modern synthetical routes.

Acknowledgment. This work was financially supported by the Deutsche Forschungsgemeinschaft (SFB 481). The authors appreciate stimulating discussions with G. Hadziioannou.

References and Notes

(1) Henkee, C. S.; Thomas, E. L.; Fetters, L. J. *J. Mater. Sci.* **1988**, *23*, 1685.
(2) Russell, T. P.; Coulon, G.; Deline, V. R.; Miller, D. C. *Macromolecules* **1989**, *22*, 4600.
(3) Collin, B.; Chatenay, D.; Coulon, G.; Aussere, D.; Gallot, Y. *Macromolecules* **1992**, *25*, 1621.
(4) Mayes, A. M.; Russell, T. P.; Bassereau, P.; Baker, S. M.; Smith, G. S. *Macromolecules* **1994**, *27*, 749.
(5) Carvalho, B. L.; Thomas, E. L. *Phys. Rev. Lett.* **1994**, *73*, 3321.
(6) Kramer, E. J.; Schwarz, S. A.; Gebizlioglu, O.; Sinha, S. K. *Macromolecules* **1994**, *27*, 4000.
(7) Grim, P. C. M.; Nyrkova, I. A.; Semenov, A. N.; ten Brinke, G.; Hadziioannou, G. *Macromolecules* **1995**, *28*, 7501.
(8) Krausch, G. *Mater. Sci. Eng.* **1995**, *R14*, 1.
(9) Mansky, P.; Russell, T. P.; Hawker, C. J.; Pitsikalis, M.; Mays, J. *Macromolecules* **1997**, *30*, 6810.
(10) Kim, G.; Libera, M. *Macromolecules* **1998**, *31*, 2169.
(11) Kim, G.; Libera, M. *Macromolecules* **1998**, *31*, 2670.
(12) Yokoyama, H.; Kramer, E. J.; Rafailovich, M. H.; Sokolov, J.; Schwarz, S. A. *Macromolecules* **1998**, *31*, 8826.
(13) Ruzette, A.-V.; Banerjee, P.; Mayes, A. M.; Pollard, M.; Russell, T. P.; Jerome, R.; Slawecki, T.; Hjelm, R.; Thiyagarajan, P. *Macromolecules* **1998**, *31*, 8509.
(14) Pickett, G. T.; Balazs, A. C. *Macromol. Theory Simul.* **1998**, *7*, 249.
(15) Huang, E.; Pruzinsky, S.; Russell, T. P.; Mays, J.; Hawker, C. J. *Macromolecules* **1999**, *32*, 5299.
(16) Mansky, P.; Tsui, O. K. C.; Russell, T. P.; Gallot, Y. *Macromolecules* **1999**, *32*, 4832.
(17) Binder, K. *Adv. Polym. Sci.* **1999**, *138*, 1.
(18) Yokoyama, H.; Kramer, E. J.; Fredrickson, G. H. *Macromolecules* **2000**, *33*, 2249.
(19) Liu, Y.; Zhao, W.; Zheng, X.; King, A.; Singh, A.; Rafailovich, M. H.; Sokolov, J.; Dai, K. H.; Huang, E.; Mansky, P.; Russell, T. P.; Harrison, C.; Chaikin, P. M.; Register, R. A.; Hawker, C. J.; Mays, J. *Macromolecules* **2000**, *33*, 80.
(20) Fasolka, M. J.; Banerjee, P.; Mayes, A. M.; Pickett, G.; Balazs, A. C. *Macromolecules* **2000**, *33*, 5702.
(21) Rehse, N.; Knoll, A.; Konrad, M.; Magerle, R.; Krausch, G. *Phys. Rev. Lett.* **2001**, *87*, 035505.
(22) Huinink, H. P.; Brokken-Zijp, J. C. M.; van Dijk, M. A. *J. Chem. Phys.* **2000**, *112*, 2452.
(23) Rockford, L.; Mochrie, S. G. J.; Russell, T. P. *Macromolecules* **2001**, *34*, 1487.
(24) Mansky, P.; Chaikin, P.; Thomas, E. L. *J. Mater. Sci.* **1995**, *30*, 1987.
(25) Park, M.; Harrison, C.; Chaikin, P. M.; Register, R. A.; Adamson, D. H. *Science* **1997**, *276*, 1401.
(26) Spatz, J. P.; Herzog, T.; Mössmer, S.; Ziemann, P.; Möller, M. *Adv. Mater.* **1999**, *11*, 149.
(27) Meiners, J.-C.; Quintel-Ritzi, A.; Mlynek, J.; Elbs, H.; Krausch, G. *Macromolecules* **1997**, *30*, 4945.
(28) The morphologies of block copolymer bulk samples that are prepared from solution show a dependence on the solvent and solvent extraction speed, too. Often the experimental conditions (solvent extraction speed, selectivity of the solvent, etc.) are rarely controlled nor quantitatively known, though.
(29) Amphiphile ABC-Dreiblockcopolymere aus Styrol, Vinylpyridin und tert-Butylmethacrylat/Methacrylsäure. E. Giebeler Dissertation, Universität Mainz, 1996.
(30) Si wafers were purchased from Crystec (Berlin, Germany).
(31) Tassin, J. F.; Siemens, R. L.; Tang, W.; Hadziioannou, G.; Swalen, J. D.; Smith, B. A. *J. Phys. Chem.* **1989**, *93*, 2106.
(32) Breiner, U.; Krappe, U.; Abetz, V.; Stadler, R. *Macromol. Chem. Phys.* **1997**, *198*, 1051. Krappe, U.; Stadler, R.; Voigt-Martin, I.-G. *Macromolecules* **1995**, *28*, 4558.
(33) Elbs, H.; Drummer, C.; Abetz, V.; Hadziioannou, G.; Krausch, G. *Macromolecules* **2001**, *34*, 7917.
(34) For the simulation the program TEMsim 1.6 developed by J. Hoffman was used. For reference, see (http://www.msri.org/publications/sgp/jim/software/temsim/index.html).
(35) Thomas, E. L.; Alward, D. B.; Kinning, D. J.; Martin, D. C.; Handlin, D. L., Jr.; Fetters, L. J. *Macromolecules* **1986**, *19*, 2197.
(36) Hasegawa, H.; Tanaka, H.; Yamasaki, K.; Hashimoto, T. *Macromolecules* **1987**, *20*, 1651.
(37) Shibayama, M.; Hashimoto, T.; Kawai, H. *Macromolecules* **1983**, *16*, 1434.
(38) Sadron, C.; Gallot, B. *Makromol. Chem.* **1973**, *164*, 301.
(39) Huang, C.-I.; Lodge, T. P. *Macromolecules* **1998**, *31*, 3556.
(40) Elbs, H. Dissertation, Universität Bayreuth, 2001.
(41) Rancon, Y.; Charvolin, J. *J. Phys. Chem.* **1988**, *92*, 2646.
(42) Goldacker, T.; Abetz, V. *Macromolecules* **1999**, *32*, 5165. Abetz, V.; Goldacker, T. *Macromol. Rapid Commun.* **2000**, *21*, 16.

MA011734E